

# Analysis of Magnetometer Data from a Strong G3 Geomagnetic Disturbance

Jessica L. Wert, Pooria Dehghanian, Anna Zhang, Melvin Stevens, Rhett Guthrie,  
Jonathan Snodgrass, Komal S. Shetye, Thomas J. Overbye, Katherine R. Davis  
*Department of Electrical and Computer Engineering*  
*Texas A&M University*  
College Station, TX

{jwert; pooria.dehghanian; a-zhang; mrstevens; rhett.guthrie;  
snodgrass; shetye; overbye; katedavis}@tamu.edu

Jennifer Gannon  
*Computational Physics, Inc*  
Boulder, CO  
gannon@cpi.com

**Abstract**—Measuring the changes to the earth’s magnetic field during geomagnetic disturbance (GMD) events provides valuable insights which can be used to better understand potential impacts of GMDs on the electrical power grid and develop mitigating measures. This paper analyzes variations in the magnetic field measurement data captured from 17 magnetometers placed across the United States over the course of a strong GMD event that occurred in early November 2021. Various correlation analyses are performed based on the magnetic field measurements and time-shifted signals during four distinct scenarios (pre-storm, early-storm, peak-storm, and post-storm). The results provide a better understanding of the changes in magnetic field patterns, which can lead to a more accurate assessment of the induced electric field on the grid.

**Index Terms**—Geomagnetic disturbances, Magnetometer, Geomagnetic field, Geoelectric field.

## I. INTRODUCTION

The sun follows an approximately 11-year cycle in which solar activity, including solar flares and coronal mass ejections (CMEs), increases near the cycle’s peak followed by a reversal of the sun’s magnetic polarities by the end of each cycle [1]. Increases in solar activity raises the likelihood of geomagnetic disturbances (GMDs) by disrupting the earth’s magnetic field. Through the principles described in Faraday’s law of induction, the changes in the earth’s magnetic field induce an electric field over the surface of the earth.

For the purposes of power systems modeling, frequency domain techniques are usually employed as the default method of computing the induced electric fields. This involves computing the Fourier Transform of the time series magnetic field measurements to obtain the magnitude and phase of magnetic field variations. In the frequency spectrum, the induced electric field may be defined as a function of earth’s surface impedance and the magnetic field as follows,

The authors would like to gratefully acknowledge the NSF Distributed Array of Small Instruments grant, Texas University and the State of Texas Governor’s University Research Initiative (GURI) grant program for funding this work.

Copyright ©2022 IEEE. Personal use of this material is permitted. However, permission to use this material for any other purposes must be obtained from the IEEE by sending a request to [pubspermissions@ieee.org](mailto:pubspermissions@ieee.org). Presented at the Texas Power and Energy Conference, College Station, TX, February 2022.

$$E_X(\omega) = -Z(\omega) \frac{B_Y(\omega)}{\mu_0} \quad (1)$$

$$E_Y(\omega) = Z(\omega) \frac{B_X(\omega)}{\mu_0} \quad (2)$$

where  $E_X(\omega)$  is the northward electric field,  $E_Y(\omega)$  is the eastward electric field,  $B_X(\omega)$  is the northward magnetic field,  $B_Y(\omega)$  is the eastward magnetic field,  $Z(\omega)$  is the earth’s surface impedance, and  $\mu_0$  is the magnetic permeability of free space. The time series of electric field values can then be obtained by computing the inverse Fourier transform of  $E(\omega)$ ,

$$E(t) = \mathcal{F}^{-1}\{E(\omega)\} \quad (3)$$

When this electric field interacts with the electric power grid, it takes the form of a quasi-dc voltage,  $V_{dc}$ , across each transmission line. The voltage induced on a transmission line can be computed by integrating  $E$  along the incremental length of the transmission line as follows,

$$V_{dc} = \oint E \cdot dl \quad (4)$$

The induced voltages generate low-frequency geomagnetically induced currents (GICs) that are superimposed on grounded conductors such as transformers with grounded-wye connection and transmission lines feeding these transformers. Deleterious consequences to the electric power grid occur when GICs are high enough to damage power system equipment such as high-voltage transformers or disrupt protective relaying schemes.

### A. Historical GMD Events

One of the most severe and fastest-moving solar storms that struck the earth was the Carrington Event of September 1859. Some studies estimate the Carrington Event to have reached a Dst index of approximately -1760 nT while later examinations suggest the storm reached a lower Dst index of approximately -850 nT [2]. Some telegraph systems in Europe and North America were destroyed as a result of the storm [2], [3]. With the present-day electric infrastructure, a solar storm of

similar magnitude to the Carrington Event would likely cause blackouts that are continental in scale.

Another famous GMD event caused by CMEs occurred in March 1989. Hailed as the largest geomagnetic storm of the last century, the storm of March 1989 produced a Dst index of -589 nT [2]. While this storm had produced a much lower magnitude of geomagnetic depression than the Carrington storm of 1859, it occurred during the era when much of the power infrastructure in North America had matured and much of civilization was dependent on a working power network. The storm produced GICs powerful enough to generate harmonics that tripped protective systems on static VAR compensators, resulting in the collapse of the Hydro Quebec power grid and cutting power to six million customers for nine hours [4]. The economic impact was estimated to be C\$13.2 billion [4].

Historical GMD events clearly demonstrate that geomagnetic storms can have significant impact on the operation and security of the power system. A difficult question the power industry is seeking to answer is when another extreme GMD event could be expected to strike the earth and how we should prepare for such events. The Space Weather Scales for Geomagnetic Storms prepared by the Space Weather Prediction Center (SWPC) of the National Oceanic and Atmospheric Administration (NOAA) approximates the average frequency of occurrence for geomagnetic storms of varying severity levels, as shown in Figure 1. Under the Geomagnetic Storm Scales, GMDs are categorized on a scale from G1 to G5. On this scale, G1 storms are the most minor and can be associated with minor fluctuations in the grid. G5 storms are the most major and can cause widespread issues with voltage control and protective systems, equipment damage, and blackouts [5].

Scale	Descriptor	Effect on Power systems	Avg. Frequency (1 cycle = 11 years)
G5	Extreme	Widespread voltage control problems and protective system problems can occur, some grid systems may experience complete collapse or blackouts. Transformers may experience damage.	4 days per cycle
G4	Severe	Possible widespread voltage control problems and some protective systems will mistakenly trip out key assets from the grid.	60 days per cycle
G3	Strong	Voltage corrections may be required, false alarms triggered on some protection devices.	130 days per cycle
G2	Moderate	High-latitude power systems may experience voltage alarms, long-duration storms may cause transformer damage.	360 days per cycle
G1	Minor	Weak power grid fluctuations can occur.	900 days per cycle

Fig. 1. NOAA Space Weather Scales for Geomagnetic Storms [5].

## B. Magnetometer Network

Magnetometers are instruments installed on the ground that are used to measure the earth's magnetic field strength and orientation. Magnetic fields are vectors, travelling with a magnitude in a particular direction. Data collected from magnetometers is commonly represented in terms of its orthogonal ( $x$ -,  $y$ -, and  $z$ -) components.  $B_X$ ,  $B_Y$ , and  $B_Z$  correspond to the geomagnetic north-south, east-west, and vertical component of the magnetic field signal, respectively. Fluctuations in the earth's magnetic field is a key marker used to assess GMD risk. A number of these devices are installed around the world to monitor the earth's magnetic field at different geographical locations. An overview of some major magnetometer networks around the globe and their capabilities has been described in a previous study [6].

A significant challenge facing power system modeling with respect to GMD event recreation and research is the scarcity of measurements across the continental United States. Magnetometers distributed across the United States are often located thousands of miles away from one another. Such widely-spaced arrays render it difficult to capture and analyze low-grade differences and magnetic field intensification within a specific geographical area with varying geological structures. The magnitude and direction of geoelectric field generated by a change in geomagnetic field varies depending on geological structure due to differences in ground conductivity. Therefore, there is a great need to reliably monitor the earth's magnetic field from a variety of different geographical locations in order to accurately model the earth's electric field, and subsequently the GICs, at corresponding locations.

Two major magnetometer networks used in this study are the Texas A&M University Magnetometer Network (TAMUMN) and the Distributed Arrays of Small Instruments (DASI) [6], [7]. The overall goal for these networks is to address insufficiency in the prior geomagnetic field measurements by enhancing spatial coverage of magnetometers in the continental U.S. and to improve research on validating GIC calculations and hazard analysis.

The DASI magnetometer network is comprised of two magnetometer arrays that are funded by the National Science Foundation (NSF) [8], [9]. The MAGStar array (most recent ongoing project) was installed by Computational Physics, Inc (CPI), whereas the Hazard SEES array (previous project) was installed by the University of Illinois. This network contains 12 magnetometers spaced at various locations in the United States as shown in red in Figure 2.

The MAGStar magnetometer stations continuously capture the earth's magnetic field at a cadence of 1 Hz and transfer data with less than 2 s latency [10]. Data communication is encrypted and information is either transferred wirelessly to a nearby data center or through a commercial cellular network [10].

TAMUMN, a project that was completed in December 2019, includes six magnetometers all situated in the state of Texas at the following locations: The towns of Amarillo, Beaumont,



Fig. 2. Magnetometer locations within the DASI and TAMU magnetometer networks presented with red and green icons, respectively.

Beeville, Overton, Stephenville, and the Texas A&M RELLIS Campus (near Bryan) [6]. These magnetometers are shown in green in Figure 2. Details on the installation of the six magnetometers, site selection process, key components, initial data collection and analysis is described in [6]. The spatial distance between each of these magnetometers is between 232 km to 486 km apart. Locations of magnetometers were specially chosen to be near GIC monitors to supplement GIC model validation. Real-time measurements of the geomagnetic field are sampled at a cadence of 1 Hz and transmitted with a latency of less than 10 ms directly to a data center on the Texas A&M RELLIS campus [6].

## II. NOVEMBER 2021 GMD STORM OVERVIEW AND ANALYSIS FORMULATION

At 19:42 UTC on November 3, 2021 the NOAA Deep Space Climate Observatory (DSCOVR) satellite detected a CME anticipated to reach the earth. This CME arrived at the earth at 19:57 UTC on November 3 and was observed on magnetometer networks including DASI and TAMUMN. The geomagnetic disturbances were characterized at 21:24 UTC to be G1 (minor). The storm levels developed to G2 (moderate) classification by 21:46 UTC and continued escalating to reach G3 (strong) classification at 23:59 UTC on November 3, 2021 [11]. The geomagnetic disturbance continued for 3 days before subsiding on November 6, 2021.

This paper seeks to glean insights from magnetometer network measurements for the early November storm such that magnetometer measurements can be effectively used in the prediction and mitigation of the effects of future GMD events on the grid. In order to accomplish this goal, measurements from the DASI and TAMU magnetometer networks are leveraged. During this storm, the Overton magnetometer in the TAMUMN was out of service and did not collect data. Data was collected from the remaining 17 magnetometers in the DASI and TAMU networks for the event and surrounding days.

This analysis considers the x- and y-components of the magnetic field ( $B_X$ ,  $B_Y$ ) which correspond to the geomagnetic

north-south and east-west, respectively. Due to the orthogonal relationship between the magnetic field and electric field, a magnetic field pointing in the x-direction translates into an electric field in the y-direction, and vice versa. Magnetic field data from November 2-6, 2021 are utilized in the following analyses. November 2, is used as the reference case, representing a non-event day. Data from November 3, marks the beginning of the storm, and the November 4 data contains the peak of the storm. Data from November 5 and 6 are used to provide post-peak GMD storm analysis.

Correlation analysis shows the degree of similarity between the magnetic field measurements in x- and y- directions and is presented in Section III-A. The temporal relationship of magnetic field measurements at different magnetometer locations is analyzed and discussed in Section III-B.

## III. DATA ANALYSIS AND DISCUSSION

Prior to beginning data analysis, the preliminary data was pre-processed to detect and remove potential outliers. These outliers were detected using the Local Outlier Factor [12], which is an unsupervised outlier detection method that relies on the density of points within a set neighborhood. With the outliers identified for each station, day, and variable, these values were replaced using a forward fill approach. Fills were used rather than outlier removal to preserve the dimensions of the data and allow for comparison for each station at every time step.

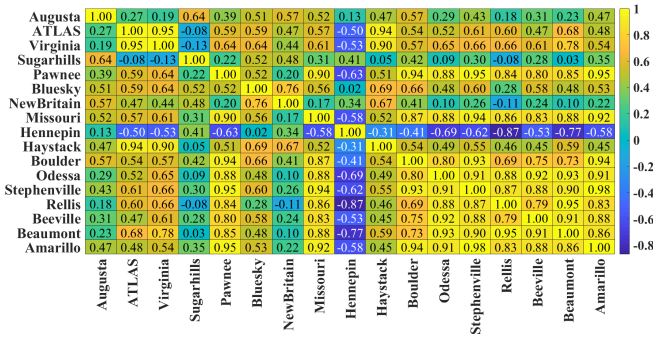
### A. Correlation Analysis

In this paper, correlation analysis is used to determine the similarity of the time-series magnetic field signals between different magnetometers. A numerical value is assigned for the result of the relationship between two quantitative variables, ranging from -1 to 1. High correlation coefficient magnitudes indicate a strong relationship between two variables. Similarly, a low correlation value is indicative of a weak relationship between two variables. Pearson's correlation coefficients are calculated in Equation 5.

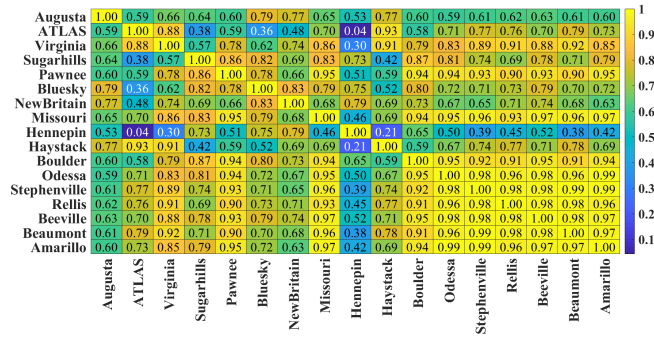
$$Corr_{A,B} = \frac{cov(A,B)}{\sigma_A \sigma_B} \quad (5)$$

where,  $cov(A,B)$  is the covariance of signals  $A$  and  $B$ , and  $\sigma_A$  and  $\sigma_B$  are the standard deviations of  $A$  and  $B$ , respectively.

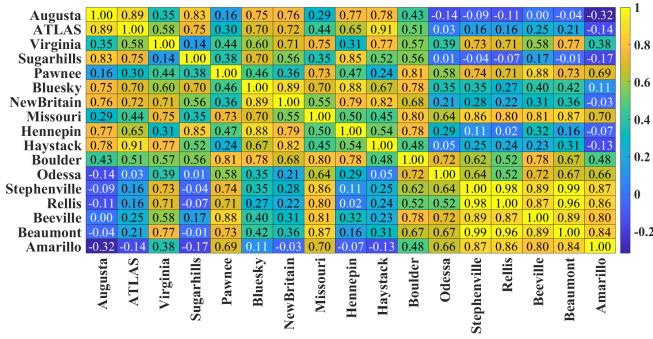
The independent variables  $A$  and  $B$  correspond to the magnetic fields recorded at different locations. Pearson's correlation coefficients are used to compare magnetic field measurements over 24-hour scenarios. The correlation study investigates four scenarios: pre-storm, storm commencement, peak-storm, and post-peak storm conditions. The magnetic field's correlation heatmap of the x-component ( $B_X$ ) and the y-component ( $B_Y$ ) between all TAMU-DASI stations in each scenario are shown in Figs. 3 and 4, respectively.



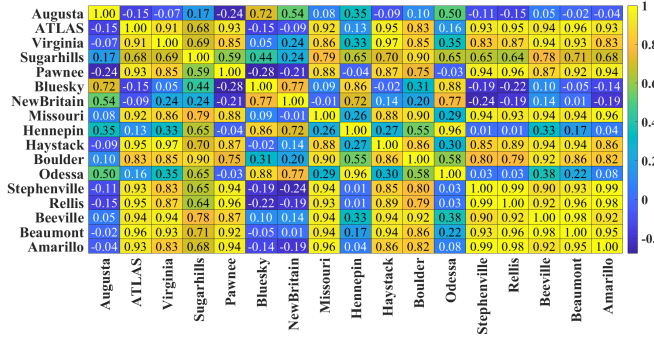
(a) Correlation of  $B_X$  on the typical pre-event day (Nov. 2).



(b) Correlation of  $B_X$  on the storm commencement day (Nov. 3).



(c) Correlation of  $B_X$  on the peak-storm day (Nov. 4).



(d) Correlation of  $B_X$  on the post-peak storm day (Nov. 5).

Fig. 3. Correlation of magnetic field ( $B_X$ ) measurements between DASI and TAMU magnetometers.

It should be noted that the Odessa magnetometer, which is part of the DASI network, is located in Texas, as is TAMUMN. The Hennepin and Sugarhills magnetometers are in Minnesota, and the Boulder and Pawnee magnetometers are in Colorado.

1) *Analysis of  $B_X$  Correlation:* On a regular (pre-storm) day, the magnetometer stations in Texas are highly correlated, as can be seen in Figure 3a. For example, Odessa has a high correlation with the magnetometers in TAMUMN. The magnetometer at Hennepin has a very low correlation (mostly negative correlation) with all other stations, and has a weak correlation of 0.4 with Sugarhills even though they are close geographically (geographic proximity shown in Fig. 2).

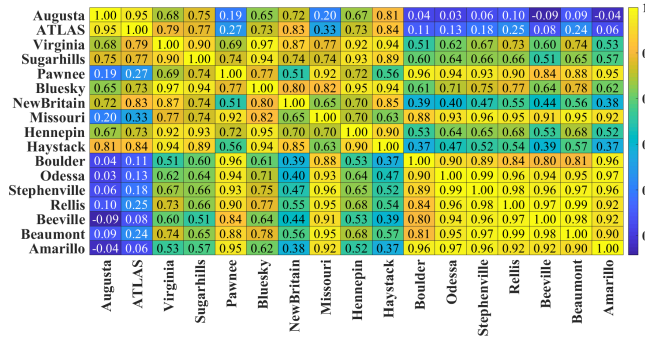
The GMD event began on Nov. 3, and the storm's peak took place in Nov. 4. As shown in Fig. 3b, the magnetic field correlation between most magnetometer stations is higher on the storm commencement day (Nov. 3) than on the pre-GMD day. The Odessa magnetometer has a higher correlation with TAMUMN compared to the pre-GMD event. Hennepin correlation with Sugarhills increases to 0.73. Odessa magnetometer has an average correlation of 0.97 to the TAMUMN.

The correlation pattern changes significantly on the peak GMD event, as illustrated in Fig. 3c. The Magnetometer at Odessa becomes less correlated with the rest of the sensors in TAMUMN. Most of the DASI magnetometers have a weaker correlation with the TAMUMN. Even the correlation among TAMUMN is lower compared to the pre-storm day. During the post-peak GMD event as shown in Fig. 3d, the correlation between Odessa and the TAMU magnetometers

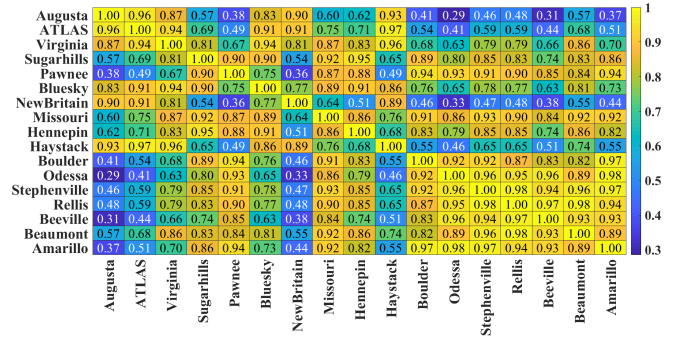
drops significantly, although they are close in terms of geographical and magnetic latitude. However, the correlation between TAMUMN restores its value in pre-storm day.

2) *Analysis of  $B_Y$  Correlation:* Fig. 4 illustrates the correlation of  $B_Y$  across TAMU and DASI magnetometers during different event days. The overall magnetic correlation has been improved during the pre-GMD event except for Augusta and Atlas stations. As it can be seen in Fig. 4a, Hennepin's  $B_Y$  correlation to the rest of the magnetometers is much higher compared to its  $B_X$  correlation (see Fig. 3a). Even the  $B_Y$  correlation is greater between TAMUMN compared to their corresponding  $B_X$  correlation values. During the storm commencement day (Nov. 3rd), the  $B_Y$  correlations of Augusta and Atlas are improved compared to the pre-storm day, however,  $B_Y$  correlations for Augusta, Atlas, New Britain, and Haystack are decreased compared to their corresponding  $B_X$  correlation values (see Fig. 3b). One can see in Fig. 4c that the  $B_Y$  correlation values are quite higher during the peak-storm day and are slightly reduced in post-peak storm day shown in Fig. 4d. Odessa's  $B_Y$  correlation to TAMUMN sensors is considerably higher in values compared to its corresponding  $B_X$  correlation.

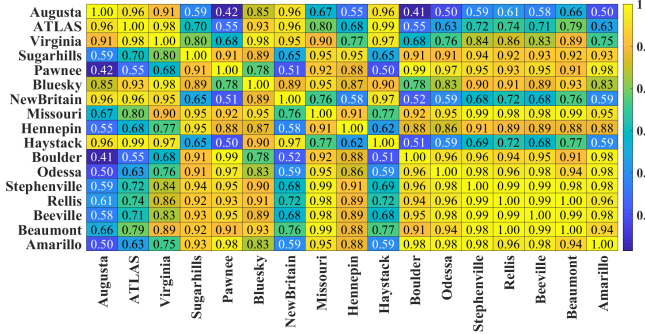
The above analysis highlights that magnetic storm variations in x- and y- directions do not follow a specific pattern and are usually more spatially spread out. The results indicate that the magnetometers are more spatially correlated in y-direction than in the x-direction. Although it is currently unclear what causes these fluctuations in the magnetic field



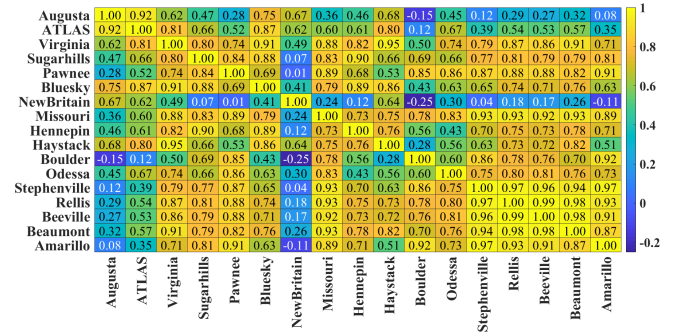
(a) Correlation of  $B_Y$  on the typical pre-event day (Nov. 2).



(b) Correlation of  $B_Y$  on the storm commencement day (Nov. 3).



(c) Correlation of  $B_Y$  on the peak-storm day (Nov. 4).



(d) Correlation of  $B_Y$  on the post-peak storm day (Nov. 5).

Fig. 4. Correlation of magnetic field ( $B_Y$ ) measurements between DASI and TAMU magnetometers.

data correlations, future research will explore possible causes for these phenomena.

### B. Cross-Correlation Analysis

Cross-correlation analysis can provide insights into the degree of similarity between two time-shifted signals. In practice, it involves the calculation of the Pearson correlation coefficient of two signals. This calculation is then repeated for each lag, or time step shift, of the signals relative to one another. The Pearson's coefficient presented in Section III-A yields the value from cross-correlation at time lag 0.

This analysis was performed on the  $B_X$  and  $B_Y$  measurements for the date range of November 2-6, 2021. This analysis shows that, between many combinations of the stations, the maximum correlation values were calculated at lag of 0. Other station pairs, however, indicated that the magnetic field measurements were more correlated with a small time lag.

As some pairs were showing that the signals were more correlated with a small time lag, the measurement signals were partitioned based on each phase of the storm events. These phases included pre-storm, G1, G2, and G3 according to the event timing from [11]. The results from these phases were filtered to highlight the station pairings at each stage of the storm that meet the following criteria:

- demonstrate improved correlation at nonzero time lags,
- correlation at optimal time lag of at least 0.80.

Table I demonstrates the prevalence of improvements to  $B_X$  signal correlation with time shifts ranging from 1 second to approximately 90 minutes. Table II shows the counts of magnetometer station pairings with higher correlation coefficients with a time shift applied to the  $B_Y$  signals. The lags at which already highly correlated stations showed an increase in their correlation have been recorded, ranging from 1 second to approximately 15 minutes.

TABLE I  
 $B_X$  MEASUREMENTS MEETING CRITERIA.

	Pre-Storm	G1	G2	G3
Pairing instances	33	41	53	17
Non-zero lag range (s)	1-5554	1-28	1-14	1-17
Improvement range (%)	0-35.25	0-8.56	0-3.40	0-0.04

TABLE II  
 $B_Y$  MEASUREMENTS MEETING CRITERIA.

	Pre-Storm	G1	G2	G3
Pairings instances	54	4	10	70
Non-zero lag range (s)	1-902	1-4	1-6	1-186
Improvement range (%)	0-3.64	0.1-1.97	0.01-0.47	0-0.75

1) *Analysis of  $B_X$  Correlation:* Table I presents the counts of already strong, yet improved correlation coefficients when comparing time-shifted signals for  $B_X$ . The x-component of the magnetic field measurements in the pre-storm section displayed improved correlation at a time lag of approximately

90 minutes. The station pairings in the pre-storm data with strong yet improved correlation at lags greater than 1 hour include Pawnee-Virginia (35.25% improved), Rellis-Virginia (19.89% improved), Rellis-Atlas (17.59% improved), Odessa-Virginia (10.82% improved), and Beaumont-Virginia (2.21% improved) (all long-distance pairings). Note that the first station mentioned in each pairing is the station to which the time-shift is applied. The G1 phase of the storm demonstrated improved correlation by about 2% at a 28 second lag when comparing the  $B_X$  signals for Beeville and Augusta. The G2 phase of the storm demonstrated increased correlation of  $B_X$  signals up to a lag of 14 seconds for the Haystack-Pawnee pairing (3% improvement in correlation at this time lag). The G3 portion of the storm demonstrated high correlation improved marginally (<1% improvement) by applying time shifts to the  $B_X$  signal up to 17 seconds for the Stephenville-Virginia and Rellis-Virginia pairs. The only station pairing that met the filtering conditions of correlation of at least 0.80 demonstrating increased correlation at non-zero lags for the  $B_X$  measurements for all phases of the event is Missouri-Beaumont. This pairing produced maximum correlation values at different time lags for each stage of the storm.

2) *Analysis of  $B_Y$  Correlation:* Table II presents the counts of already strong, yet improved correlation coefficients when comparing time-shifted signals for  $B_Y$ . The pre-storm  $B_Y$  signals demonstrated increased correlation for some pairings with lags of approximately 15 minutes. The pairings with improved correlations at lags greater than 10 minutes were Sugarhills-Atlas (3.64% improvement), Amarillo-Beaumont (1.86% improvement), and Sugarhills-Haystack (<1% improvement). For the G1 stage of the storm, the  $B_Y$  signals showed increased correlation with time shifts for only four stations with the lags of improvement ranging from 1 to 4 seconds. For the G1 stage, the pairing with the improved correlation at the longest lag was Bluesky-Stephenville (1.97% improvement). The G2 phase of the storm showed marginal improvements (<1%) for time-shifted  $B_Y$  signals with a maximum lag time of 6 seconds reported for the Hennepin-Pawnee pairing (mid-range geographic distance). The G3 portion of the storm had 70 magnetometer pairings with improved correlation when applying time shifts. The lags for this phase of the storm which yielded the highest correlation were over 3 minutes. The pairings with the longest lags (over 2 minutes) for improved correlation include Stephenville-Virginia, Sugarhills-Virginia, Sugarhills-Bluesky, Virginia-Augusta, Bluesky-Augusta, and Virginia-New Britain. The correlation improvements were marginal (<1%) for each. There was no station pairing that met the filtering conditions for all phases of the storm.

Some signals showing greater correlation with time-shifted signals from other stations may indicate a possibility of using the signal from one location to give warnings before similar changes to the magnetic field are observed at other stations. A longer lead-time or increased confidence in the variation of the magnetic field could provide power engineers additional time to determine or enact mitigation efforts. This correlation relationship observed was not strongly consistent throughout

the phases of the storm. Thus, further study is required to determine if the relationship between measured magnetic fields at magnetometer locations would hold for other storms.

#### IV. CONCLUSIONS

This paper has provided analysis of magnetometer measurements from the DASI and TAMU magnetometer networks for a GMD which occurred in early November, 2021. This geomagnetic storm began as a G1 (minor) event and, over the course of about two and a half hours, escalated to a G3 (strong) event. The similarities in magnetic field variations have been studied by analyzing the correlation between station measurements for different days of the event and evaluating the time-shifted correlation.

The results of the paper suggest that some magnetometers have strong similarities in terms of magnetic variations even though they are located widely apart, and further statistical analyses are needed to generalize the findings. Simulated results of time-shifted simulations provide insight into changes in magnetic variation patterns between magnetometers that can serve as an indicator for other magnetometers. With this technique, the magnetic field can be monitored at one location to give early warning of similar changes in the magnetic field at another site.

#### REFERENCES

- [1] D. H. Hathaway, "The solar cycle," *Living Reviews in Solar Physics*, vol. 7, no. 1, 2010. [Online]. Available: <https://link.springer.com/content/pdf/10.12942%2Flrsp-2010-1.pdf>
- [2] D. N. Baker, X. Li, A. Pulkkinen, C. M. Ngwira, M. L. Mays, A. B. Galvin, and K. D. C. Simunac, "A major solar eruptive event in July 2012: Defining extreme space weather scenarios," *Space Weather*, vol. 11, no. 10, pp. 585–591, 2013. [Online]. Available: <https://agupubs.onlinelibrary.wiley.com/doi/pdf/10.1002/swe.20097>
- [3] "Geomagnetic disturbance monitoring approach and implementation strategies," U.S. Department of Energy, Report, 2019.
- [4] "Solar storm risk to the north american electric grid," Lloyd's and the Atmospheric and Environmental Research, Inc., Report, 2013.
- [5] "NOAA space weather scales." [Online]. Available: <https://www.swpc.noaa.gov/noaa-scales-explanation>
- [6] K. S. Shetye, R. R. Kumar, C. Klauber, Z. Mao, T. J. Overbye, J. Gannon, and M. Henderson, "Development and electric grid applications of a magnetometer network," *IEEE Open Access Journal of Power and Energy*, vol. 8, pp. 77–84, 2021.
- [7] N. R. Council, *Distributed Arrays of Small Instruments for Solar-Terrestrial Research: Report of a Workshop*. Washington, DC: The National Academies Press, 2006. [Online]. Available: <https://www.nap.edu/catalog/11594/distributed-arrays-of-small-instruments-for-solar-terrestrial-research-report>
- [8] J. Gannon and D. Knipp, "Dasi track 2: Magstar- improving the spatial coverage of united states magnetometers for space weather research and operations," 2019. [Online]. Available: [https://www.nsf.gov/awardsearch/showAward?AWD\\_ID=\\$1933040](https://www.nsf.gov/awardsearch/showAward?AWD_ID=$1933040)
- [9] J. Makela, J. Sebestik, K. Davis, H. Zhu, and T. Overbye, "Hazards sees: Improved prediction of geomagnetic disturbances, geomagnetically induced currents, and their impacts on power distribution systems," 2015. [Online]. Available: [https://www.nsf.gov/awardsearch/showAward?AWD\\_ID=\\$1520864&HistoricalAwards=\\$false](https://www.nsf.gov/awardsearch/showAward?AWD_ID=$1520864&HistoricalAwards=$false)
- [10] "Magstar 3 magnetometer station." [Online]. Available: <https://gmd.cpi.com/MagSTAR3Datashet.pdf>
- [11] "G3 (strong) geomagnetic storm conditions reached with cme arrival," Nov 2021. [Online]. Available: <https://www.swpc.noaa.gov/news/g3-strong-geomagnetic-storm-conditions-reached-cme-arrival>
- [12] M. M. Breunig, H.-P. Krieger, R. T. Ng, and J. Sander, "Lof: Identifying density-based local outliers," *SIGMOD Rec.*, vol. 29, no. 2, p. 93–104, may 2000. [Online]. Available: <https://doi.org/10.1145/335191.335388>